Microwave Thawing of Cylinders

B. J. Pangrle, K. G. Ayappa, and H. T. Davis
Dept. of Chemical Engineering and Materials Science, University of Minnesota, Minneapolis, MN 55455

E. A. Davis and J. Gordon
Dept. of Food Science and Nutrition, University of Minnesota, St. Paul, MN 55108

The finite element method was used to model microwave thawing of pure-water and 0.1-M NaCl cylinders. The electromagnetic field was described by Maxwell's equations with temperature-dependent dielectric properties, while the heat equation, coupled with the Stefan and Robin conditions, was used to describe the thawing process. An additional equation for the frozen volume fraction was used, when necessary, to account for the presence of a mushy region. Two microwave frequencies, 915 MHz and 2,450 MHz, were examined and the microwave radiation was assumed to be radially isotropic and normal to the surface of the cylinder. Results show that a two-phase mushy region may exist, and an additional thawing front may appear at the center of the cylinder. Salt cylinders have a higher dielectric loss than pure-water cylinders and therefore thaw more quickly. Internal resonance occurs when the wavelength of the radiation is a harmonic of the cylinder radius. Resonance increases power deposition and expedites the thawing process. The onset of resonance alters thawing times and complicates the development of heuristic rules for microwave thawing.

Introduction

Heating lossy dielectric media by electromagnetic (EM) radiation has found widespread use in commercial and industrial applications. These applications rely on internal heat generation produced from interactions between the media and the EM radiation. Many governments have imposed strict regulations on which frequencies may be used for industrial, scientific and medical use (Varey, 1990). In North America the microwave frequencies of 915 MHz and 2,450 MHz are available and in the British Isles 896 MHz and 2,450 MHz, while there is no frequency allocated near 900 MHz in continental Europe (Pearce, 1990). In the U.S., 915 MHz is used commonly in industrial ovens and 2,450 MHz in household ovens. Heating is different at these two frequencies. The longer wavelength (915 MHz) radiation penetrates deeper into the sample and distributes power more evenly. The shorter wavelength (2,450 MHz) radiation allows for more node/antinode formation within the oven capacity and sample. At a node the electric field is zero and no power is deposited, whereas at an antinode there is a peak in the power deposition.

A process common to industry and household applications is microwave thawing. The EM phenomenon associated with ice/water systems is also a concern to scientists studying the cryosphere (Vant et al., 1978; Mätzler and Wegmüller, 1987) and attenuation of radar signals in the atmosphere (Sihvola, 1989; Klassen, 1990). Thawing rates for frozen samples depend on the sample's material properties and dimensions and the magnitude and frequency of the electromagnetic radiation. For example, consider a frozen cylinder placed in an environment whose temperature is above the cylinder's freezing point. At first, the phase-change front moves inward from the surface. Exposing this thawing cylinder to a radially symmetric EM field accelerates the progress of the phase-change front. Additionally, another phase-change front may appear at the cylinder's center (due to the presence of an antinode or focusing), and/or thawing of the frozen region may occur resulting in a heterogeneous region of frozen and thawed phases. This region is commonly referred to as a "mushy" region.

Most classical solutions to phase-change or "Stefan" problems do not consider internal heat generation or mushy regions. If a "mushy" region exists, it is usually due to impurities that cause the phase change to occur over a temperature range. In some instances, the mushy region can be ignored and replaced by a sharp moving interface that is at a discrete transition temperature (Özisik, 1980). The validity of this simplification

depends on the temperature range being small compared to the overall temperature span. For a frozen sample exposed to microwave radiation, the theoretical analysis is more complex. Internal heat generation must be accounted for, and the presence of multiple fronts and mushy regions may alter total thawing times significantly.

Coleman (1990) solved analytically the classical Stefan model for phase change using Lambert's law to approximate the field equations. Lambert's law is a simplification to the EM field equations which cannot account for node/antinode formation (Ayappa et al., 1991a). Coleman's results for microwave illumination of a semi-infinite slab showed that *superheating* (a rise in the temperature of the frozen region above the melting point) is possible. Coleman then eliminated the *superheated* region and used the *enthalpy* method formulation, which allows for a mushy region. A mushy region was also considered by Taoukis et al. (1987), who modeled microwave thawing of slabs and cylinders. Their equation describing the mushy region accounted for power being consumed as latent heat which decreased the frozen fraction in the isothermal, $T = T_{\text{melt}}$ region. They also varied the dielectric properties in this region according to the changing frozen fraction. Their work, based on the modified isotherm migration method (MIMM) and solved by finite differences, also used Lambert's law to simplify the problem. In another approach, Pangrle et al. (1991) allowed for slight *superheating* in the frozen region. They solved Maxwell's equations analytically and the heat equation numerically. Their study, as well as the studies mentioned previously, assumed that the dielectric properties were independent of temperature. Ayappa et al. (1991b) have studied the case of temperature-dependent properties.

Mathematical models of the microwave heating process should account for phenomena such as node/antinode formation, phase change (thawing and evaporation), and material property changes that occur with respect to temperature (Datta, 1990). Previous studies have not met all of these criteria and therefore lack an adequate description of the physical situation. To develop a more complete model, we have examined the melting of pure and 0.1-M NaCl ice/water cylinders ($R = 1.0$, 2.0 and 3.0 cm) exposed to 915-MHz and 2,450-MHz radiation. Maxwell's equations were used to describe the EM phenomena. The heat equation with an internal heat generation term coupled with the Stefan and Robin conditions was used to describe heat transfer, while the method used by Taoukis et al. was used to describe the mushy region. The system of equations was solved using Galerkin finite elements and Newton iteration techniques. Nonlinearity arises due to the Stefan condition, the frozen fraction and the temperature dependence of the dielectric properties, whose behavior was taken from previous literature. The simulation results provided transient temperature profiles, power profiles, and thawing front position(s). Results are summarized as final thawing times in regard to the composition, geometry and incident power.

Theory

Heat equation

Heat conduction in the media is described as follows:

$$\rho C_p \frac{\partial T}{\partial t} = \nabla \cdot (k \nabla T) + p(\mathbf{r}, t), \tag{1}$$

where ρ, C_p, and k are the density, heat capacity, and thermal conductivity, respectively. The power term $p(\mathbf{r}, t)$ is determined from the real and imaginary components of the EM field.

The Robin condition is used at the surface of the cylinder:

$$\boldsymbol{n} \cdot (k_t \nabla T_s) = -h(T_s - T_\infty), \tag{2}$$

where h is the heat transfer coefficient and $\boldsymbol{n}$ is the unit normal vector. The boundary between the thawed and frozen region for a front moving in the negative z direction is described by the Stefan equation:

$$-\boldsymbol{n} \cdot (k_f \nabla T_f) + \boldsymbol{n} \cdot (k_t \nabla T_t) = -\rho \lambda \frac{ds}{dt}, \tag{3}$$

where λ is the latent heat of fusion.

Finally, the equation describing the "mushy" region (Taoukis, 1987), should it exist, is:

$$\frac{d}{dt}\int_V \{\rho_t H_t [1 - \varphi(r, t)] + \rho_f H_f \varphi(r, t)\} dV = \int_V p(r, t) dV, \tag{4}$$

where V is the volume of the mushy region, and H_t and H_f are the enthalpies of the thawed and frozen phases, respectively. For a single front, the integration is from the center to the phase-change front. If two fronts are present, the integration is from the inner front to the outer one. In Eq. 4, $\rho\lambda$ replaces $\rho_t H_t - \rho_f H_f$ if ρH is constant in each phase.

Wave propagation

A propagating electromagnetic wave is composed of oscillating electric ($\boldsymbol{E}$) and magnetic ($\boldsymbol{H}$) field components. Maxwell's equations describing their space and time dependence are:

$$\nabla \times \boldsymbol{E} = -\frac{\partial \boldsymbol{B}}{\partial t}$$

and

$$\nabla \times \boldsymbol{H} = \boldsymbol{J} + \frac{\partial \boldsymbol{D}}{\partial t}, \tag{5}$$

where $\boldsymbol{E}$ and $\boldsymbol{H}$ are the electric and magnetic fields, $\boldsymbol{J}$ the current flux, $\boldsymbol{D}$ electric displacement, and $\boldsymbol{B}$ magnetic induction. The constitutive relations relating $\boldsymbol{J}$, $\boldsymbol{D}$ and $\boldsymbol{B}$ to $\boldsymbol{E}$ and $\boldsymbol{H}$ are:

$$\boldsymbol{J} = \sigma(\omega)\boldsymbol{E}(t) \qquad \boldsymbol{D} = \epsilon(\omega)\boldsymbol{E}(t)$$

and

$$\boldsymbol{B} = \mu(\omega)\boldsymbol{H}(t), \tag{6}$$

where $\boldsymbol{E} = \overline{\boldsymbol{E}} e^{-i\omega t}$ and $\boldsymbol{H} = \overline{\boldsymbol{H}} e^{-i\omega t}$. Alternatively $e^{i\omega t}$ can be used to express the time dependence. Equations 5 and 6 yield:

$$\nabla \times \overline{\boldsymbol{E}} = i\omega\mu(\omega)\overline{\boldsymbol{H}} \tag{7}$$

and

$$\nabla \times \overline{H} = [\sigma(\omega) - i\omega\epsilon(\omega)]\overline{E} \equiv -i\omega\epsilon^*\overline{E} \tag{8}$$

where the "complex dielectric constant" ϵ^* is defined as:

$$\epsilon^*(\omega) \equiv \epsilon(\omega) + \frac{i\sigma(\omega)}{\omega} \equiv \epsilon'(\omega) + i\epsilon''(\omega). \tag{9}$$

The material's ability to store electrical energy is represented by $\epsilon' = Re(\epsilon^*)$, and $\epsilon'' = Im(\epsilon^*)$ accounts for losses through energy dissipation. The conductivity $\sigma(\omega)$, dielectric constant $\epsilon(\omega)$, and magnetic permeability $\mu(\omega)$ are in general complex functions of the frequency of the radiation ω.

Neglecting magnetic effects, the magnetic permeability $\mu(\omega)$ is approximated by its value μ_0 in free space. The time derivatives of σ and ϵ can also be neglected, since the time scale of electromagnetic propagation is much smaller than the time scales for thermal diffusion. With these assumptions and the condition of electroneutrality of the medium, which implies $\nabla \cdot (\epsilon^* \overline{E}) = 0$, Eqs. 7 and 8 can be combined to give:

$$\nabla\left(\overline{E} \cdot \frac{\nabla\epsilon^*}{\epsilon^*}\right) + \nabla^2\overline{E} + k^2\overline{E} = 0, \tag{10}$$

where

$$k^2 = \omega^2\mu_0\epsilon_0(\kappa' + i\kappa''). \tag{11}$$

The relative dielectric constant κ' and the relative dielectric loss κ'' are:

$$\kappa' \equiv \epsilon'/\epsilon_0 \quad \text{and} \quad \kappa'' \equiv \epsilon''/\epsilon_0. \tag{12}$$

To simplify the notation, the overbar on $\overline{E}$ and $\overline{H}$ will be dropped from this point on. The propagation constant k is a complex quantity

$$k = \alpha + i\beta, \tag{13}$$

where α and β are related to the dielectric properties of the medium and frequency of radiation by:

$$\alpha = \frac{2\pi f}{c}\sqrt{\frac{\kappa'(\sqrt{1+\tan^2\delta}+1)}{2}}, \tag{14}$$

and

$$\beta = \frac{2\pi f}{c}\sqrt{\frac{\kappa'(\sqrt{1+\tan^2\delta}-1)}{2}}, \tag{15}$$

where

$$\tan\delta = \frac{\kappa''}{\kappa'}. \tag{16}$$

In Eqs. 14 and 15, $c = 1/\sqrt{\mu_0\epsilon_0}$ where c is the speed of light and ω is replaced by $2\pi f$, where f is the frequency of radiation.

The phase constant α is related to the wavelength of radiation in the medium (λ_m) by:

$$\lambda_m = \frac{2\pi}{\alpha}, \tag{17}$$

which in free space reduces to $\lambda_0 = c/f$. The attenuation constant β is a rate constant for the decay of the incident field of intensity E_0. For instance, in a semi-infinite sample the interior field obeys the equation:

$$E = E_{0^e}{}^{-\beta z}. \tag{18}$$

Power dissipation

The power flux associated with a propagating electromagnetic wave is represented by the Poynting vector S and the time average flux for harmonic fields (Stratton, 1941):

$$S = \frac{1}{2}E \times H^*. \tag{19}$$

The power dissipated per unit volume is:

$$p(r) = -Re(\nabla \cdot S) = \frac{1}{2}\omega\epsilon_0\kappa''(E \cdot E^*). \tag{20}$$

Therefore, given the electric field intensity in the medium the local power dissipated is calculated by Eq. 20.

Analysis

Microwave heating in a cylinder

Consider a cylinder with radius R exposed to microwaves as shown in Figure 1. This figure illustrates a three-layer situation where the $l = 2$ layer, the mushy zone, is surrounded by two thawed layers. The sample is assumed to be homogeneous and isotropic. The surrounding medium is at ambient temperature and heat is lost by convection at the surface. If ρ_0, $C_{p,0}$, and k_0 are reference thermal properties, then dividing Eq. 1 by k_0 and using the dimensionless variables:

$$r = \frac{r^*}{R}, \qquad \theta_l = \frac{T_l - T_\infty}{T_0},$$

$$Bi = \frac{hR}{k_m}, \qquad \tau = \frac{k_0 t}{\rho_0 C_{p,0} R^2},$$

$$\mathcal{L} = \frac{\lambda}{T_0 C_{p,0}}, \qquad a = \frac{s}{R},$$

the transient one-dimensional heat conduction equation for the multilayer cylinder is:

$$\overline{\rho_l C_{p,l}}\frac{\partial\theta_l}{\partial\tau} = \frac{1}{r}\frac{\partial}{\partial r}\left(\bar{k}_l r\frac{\partial\theta_l}{\partial r}\right) + P_l(r, \tau), \tag{21}$$

for

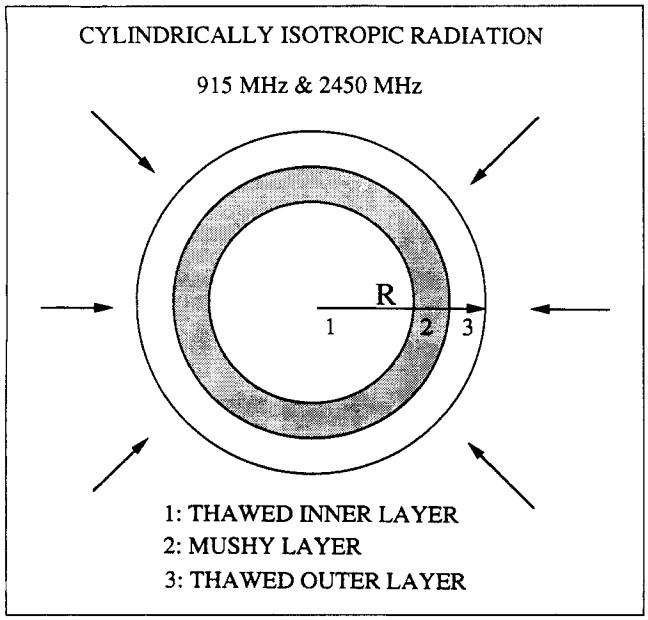

Figure 1. Frozen cylinder with EM radiation incident normal to the surface.

$$r_l \le r \le r_{l+1} \quad \text{and} \quad l = 1..m,$$

where

$$P_l = \frac{p_l R^2}{k_0 T_0}, \quad \overline{P_l C_{p,l}} = \frac{P_l C_{p,l}}{\rho_0, C_{p,0}} \quad \text{and} \quad \bar{k}_l = \frac{k_l}{k_0}.$$

The temperature and power in the lth layer are θ_l and P_l, respectively. The boundary conditions are:

$$\frac{\partial \theta_1}{\partial r} = 0 \quad \text{at} \quad r = r_1 = 0,$$

and (22)

$$\frac{\partial \theta_m}{\partial r} + Bi\theta_m = 0 \quad \text{at} \quad r = r_{m+1} = 1.$$

The initial condition is:

$$\theta(\tau = 0) = \theta_0 \quad \text{for} \quad 0 \le r \le 1. \tag{23}$$

The microwave power term is a function of temperature and is obtained by solving Maxwell's equations simultaneously with Eq. 21.

The Stefan condition for the front moving in the negative r direction at $a = a_{l+1}$ is:

$$-\mathcal{L}\frac{da_l}{d\tau} = \bar{k}_{l+1}\frac{\partial \theta_{l+1}}{\partial r} - \bar{k}_l \frac{\partial \theta_l}{\partial r}, \tag{24}$$

and the condition for the front moving in the positive r direction at $a = a_l$ is:

$$\mathcal{L}\frac{da_l}{d\tau} = \bar{k}_l \frac{\partial \theta_l}{\partial r} - \bar{k}_{l-1}\frac{\partial \theta_{l-1}}{\partial r}, \tag{25}$$

where $\theta(a = a_l) = \theta(a = a_{l+1}) = \theta_{\text{melt}}$. To account for the presence of a mushy region, it is necessary to decrease the latent heat according to the frozen volume fraction, that is, multiply $\mathcal{L}$ by φ. Additionally, the gradient in the mushy region is zero since the temperature is fixed at the melting point.

The equation governing the frozen volume fraction in the mushy zone is a function of time and position:

$$-\mathcal{L}\frac{\partial \varphi(r, \tau)}{\partial \tau} = P(r, \tau). \tag{26}$$

Maxwell's equations for a cylinder

Microwaves are assumed to be incident on a cylinder as shown in Figure 1. For propagation of uniform waves in polar coordinates, the electric $E_z(r^*)$ and magnetic $H_\phi(r^*)$ components lie in a cylindrical surface of uniform intensity varying only in the direction of propagation along the radial r^* – axis. The wave equation, Eq. 10, is:

$$\frac{d^2 E_{z,l}}{dr^{*2}} + \frac{1}{r^*}\frac{dE_{z,l}}{dr^*} + k_l^2 E_{z,l} = 0, \tag{27}$$

for

$$r_l^* \le r^* \le r_{l+1}^* \quad \text{and} \quad l = 1...m,$$

where $k_l^2 = \omega^2 \mu_0 \epsilon_0 [\kappa_l' + i\kappa_l'']$, and $E_{z,l}$, are the propagation constant and electric field intensity in the lth layer, respectively. The number of layers depends on the number of fronts. It is important to note that the dielectric properties in the mushy region depend on φ, and in the thawed and frozen layers κ' and κ'' depend on θ.

To derive the radiation boundary condition, the field outside the cylinder is expressed in terms of waves traveling in opposite directions (Balanis, 1989):

$$E_{z,l}(r^*) = C_1 H_0^{(1)}(kr^*) + E_0 H_0^{(2)}(kr^*), \tag{28}$$

where $H_0^{(1)}$ and $H_0^{(2)}$ are Hankel functions of the first and second kind, respectively, and E_0 is the intensity of the incident radiation. The constant C_1 is obtained by evaluating the field at $r^* = R$, the surface of the cylinder. Taking the derivative of Eq. 28 with respect to position leads to the radiation boundary condition,

$$\frac{dE_{z,l}}{dr^*} + \alpha_0 E_{z,l}\frac{H_1^{(1)}(\alpha_0 R)}{H_0^{(1)}(\alpha_0 R)} = -\frac{i4E_0}{\pi R H_0^{(1)}(\alpha_0 R)} \quad \text{at} \quad r^* = R \tag{29}$$

and at the center of the cylinder

$$\frac{dE_{z,l}}{dr^*} = 0 \quad \text{at} \quad r^* = 0,$$

where α_0 is the free space wave number. The intensity of the incident field P_0 is related to E_0 by:

$$P_o(r^*) = \frac{c\epsilon_0 E_0^2}{\pi \alpha_0 r^*}.$$

The Maxwell equations are rendered dimensionless by substituting the relationships:

$$r = \frac{r^*}{R} \quad \text{and} \quad u_l = \frac{E_{z,l}}{E_0}.$$

Noting that $u_l = v_l + iw_l$, Eq. 26 reduces to the following two equations which are solved with their appropriate boundary conditions:

$$\frac{d^2 v_l}{dr^2} + \frac{1}{r}\frac{dv_l}{dr} + \psi_l v_l - \chi_l w_l = 0 \tag{30}$$

and

$$\frac{d^2 w_l}{dr^2} + \frac{1}{r}\frac{dw_l}{dr} + \psi_l w_l + \chi_l v_l = 0, \tag{31}$$

where $\psi_l = R^2\omega^2\mu_0\epsilon_0\kappa_l'(\varphi, \theta)$ and $\chi_l = R^2\omega^2\mu_0\epsilon_0\kappa_l''(\varphi, \theta)$. The dielectric properties in the mushy region depend on φ and are approximated by the formula:

$$\kappa_{\text{mushy}}(\varphi) = \frac{\kappa_f[\kappa_t(2-\varphi) + \kappa_f\varphi]}{\kappa_f(2-\varphi) + \kappa_t\varphi}, \tag{32}$$

(Taoukis et al., 1987) for $\varphi = 1$, $\kappa_{\text{mushy}} = \kappa_f$. Since the thawing is isothermal, there is no need to adjust k and C_p.

The boundary conditions at $r = 0$ are:

$$\frac{dv_1}{dr} = \frac{dw_1}{dr} = 0 \tag{33}$$

while the conditions at $r = 1$ are:

$$\frac{dv_m}{dr} + c_1 v_m + c_2 w_m = -\frac{4}{\pi}\frac{Y_0(\alpha_0 R)}{J_0^2(\alpha_0 R) + Y_0^2(\alpha_0 R)} \tag{34}$$

and

$$\frac{dw_m}{dr} + c_1 w_m - c_2 v_m = -\frac{4}{\pi}\frac{J_0(\alpha_0 R)}{J_0^2(\alpha_0 R) + Y_0^2(\alpha_0 R)}. \tag{35}$$

where

$$c_1 = R\alpha_0\left[\frac{J_1(\alpha_0 R)J_0(\alpha_0 R) + Y_1(\alpha_0 R)Y_0(\alpha_0 R)}{J_0^2(\alpha_0 R) + Y_0^2(\alpha_0 R)}\right] \quad \text{and}$$

$$c_2 = \frac{2}{\pi[J_0^2(\alpha_0 R) + Y_0^2(\alpha_0 R)}$$

The power is calculated from v_l and w_l:

$$P_l(r, \tau) = \frac{R^2\omega\epsilon_0\kappa_l'' E_0^2}{k_0 T_0}(v_l^2 + w_l^2) \quad \text{for} \quad l = 1 \ldots m. \tag{36}$$

Finite element analysis

The Galerkin finite element method is used to solve the coupled nonlinear equations (Eqs. 21, 26, 30 and 31) with their respective interface and boundary conditions. For a general equation of the form:

$$Lu = f, \tag{37}$$

Galerkin finite elements expands the unknown, u in a finite element basis set $\{\phi\}$. Thus,

$$u \approx \tilde{u} = \sum_{j=1}^{N} u_j \phi_j(z). \tag{38}$$

The error, $L\tilde{u} - f$, is set orthogonal to the basis functions, and

$$\int_0^1 (L\tilde{u} - f)\phi_i dz = 0, \tag{39}$$

for

$$i = 1 \ldots N.$$

Integrating by parts and incorporating boundary and interface conditions, Eq. 39 results in a set of algebraic equations whose solution yields the unknown coefficients u_j of the expansion.

Finite difference approximations are used for the time derivatives. In particular, the temperature and frozen fraction derivatives with respect to time are:

$$\frac{\partial(\theta, \varphi)}{\partial\tau} = \frac{d(\theta, \varphi)}{d\tau} - V_{\text{mesh}}\frac{\partial(\theta, \varphi)}{\partial\tau} \tag{40}$$

due to the moving coordinate system. This results in an additional time derivative for V_{mesh}, the mesh velocity. Altogether, there are four time derivatives and they are approximated by first-order finite differences:

$$\frac{d\theta}{d\tau} = \frac{\theta^{t+1} - \theta^t}{\Delta\tau}, \quad V_{\text{mesh}} = \frac{r^{t+1} - r^t}{\Delta\tau},$$

$$\frac{d\varphi}{d\tau} = \frac{\varphi^{t+1} - \varphi^t}{\Delta\tau}, \quad \text{and} \quad \frac{da_l}{d\tau} = \frac{a_l^{t+1} - a_l^t}{\Delta\tau},$$

where the $da/d\tau$ term appears once for each front. The mesh velocity term contains no independent unknowns and depends on the unknown front position(s). The mesh coordinates, as a function of front position, are for a three-region, two-front situation:

$$r^{t+1} = \frac{a_1^{t+1}}{a_1^t} r^t \quad \text{for region I}$$

$$r^{t+1} = a_2^{t+1} - \frac{(a_2^{t+1} - a_1^{t+1})}{(a_2^t - a_1^t)}(r^t - a_2^t) \quad \text{for region II}$$

$$r^{t+1} = 1 - \frac{(1 - a_2^{t+1})}{(1 - a_2^t)} r^t \quad \text{for region III}$$

where a_1 and a_2 correspond to the fronts adjacent to layers 1 and 2, respectively.

Expanding the real (v_x) and imaginary components (w_x) of the electric field, temperature (θ) and the frozen fraction (φ) in the basis $\{\phi\}$,

$$\tilde{v}_x=\sum_{k=1}^{N} v_k\phi_k(r),\ \tilde{w}_x=\sum_{k=1}^{N} w_k\phi_k(r),$$

$$\tilde{\theta}=\sum_{k=1}^{N}\theta_k(\tau)\phi_k(r),\quad \text{and}\quad \tilde{\varphi}=\sum_{k=1}^{N}\varphi_k(\tau)\phi_k(r) \tag{41}$$

for

$$0\le r\le 1,$$

the Galerkin finite element method yields the following nonlinear residual equations for Eqs. 21, 30 and 31:

$$\begin{aligned}R_i^{(1)}=&\sum_{k=1}^{N} v_k^{t+1}\int_0^1\phi_i'\phi_k' r_k^{t+1}dr^{t+1}\\&-\sum_{k=1}^{N} v_k^{t+1}\int_0^1\psi^{t+1}\phi_i\phi_k r_k^{t+1}dr^{t+1}\\&+\sum_{k=1}^{N} w_k^{t+1}\int_0^1\chi^{t+1}\phi_i\phi_k r_k^{t+1}dr^{t+1}+\alpha_0 R w_N^{t+1}\delta_{iN}\\&+c_1 v_N\delta_{iN}+c_2 w_N\delta_{iN}+\frac{4}{\pi}\frac{Y_0(\alpha_0 R)}{J_0^2(\alpha_0 R)+Y_0^2(\alpha_0 R)}\delta_{iN},\end{aligned} \tag{42}$$

$$\begin{aligned}R_i^{(2)}=&\sum_{k=1}^{N} w_k^{t+1}\int_0^1\phi_i'\phi_k' r_k^{t+1}dr^{t+1}\\&-\sum_{k=1}^{N} v_k^{t+1}\int_0^1\chi^{t+1}\phi_i\phi_k r_k^{t+1}dr^{t+1}\\&-\sum_{k=1}^{N} w_k^{t+1}\int_0^1\psi^{t+1}\phi_i\phi_k r_k^{t+1}dr^{t+1}+\alpha_0 R v_N^{t+1}\delta_{iN}\\&+c_1 w_N\delta_{iN}-c_2 v_N\delta_{iN}+\frac{4}{\pi}\frac{J_0(\alpha_0 R)}{J_0^2(\alpha_0 R)+Y_0^2(\alpha_0 R)}\delta_{iN},\end{aligned} \tag{43}$$

and

$$\begin{aligned}R_i^{(3)}=&\sum_{k=1}^{N}\int_0^1\overline{\rho C_p}\left\{\frac{\theta_k^{t+1}-\theta_k^t}{\Delta\tau}\right\}\phi_i\phi_k r_k^{t+1}dr^{t+1}\\&-\sum_{k=1}^{N}\theta_k^{t+1}\int_0^1\overline{\rho C_p}\left\{\frac{r_k^{t+1}-r_k^t}{\Delta\tau}\right\}\phi_i\phi_k' r_k^{t+1}dr^{t+1}\\&+\sum_{k=1}^{N}\theta_k^{t+1}\int_0^1\bar{k}\phi_i'\phi_k' r_k^{t+1}dr^{t+1}\\&-\frac{R^2\omega\epsilon_0 E_0^2}{k_0 T_0}\int_0^1\kappa''^{t+1}\left\{\left(\sum_k v_k^{t+1}\phi_k\right)^2\right.\\&\left.+\left(\sum_k w_k^{t+1}\phi_k\right)^2\right\}\phi_i r_k^{t+1}dr^{t+1}\\&+\bar{k}Bi\theta_N^{t+1}\delta_{iN}.\end{aligned} \tag{44}$$

For a node on a phase-change front it is necessary to include:

$$a_l^{t+1}\mathfrak{L}\frac{a_l^{t+1}-a_l^t}{\Delta\tau}$$

in the $R^{(3)}$ residual.

The residual equation for the mushy region, Eq. 26, is:

$$\begin{aligned}R_i^{(4)}=&-\sum_{k=N_{a_l}}^{N_{a_{l+1}}}\frac{R^2\omega\epsilon_0 E_0^2}{k_0 T_0}\int_0^1\kappa''^{t+1}\left\{\left(\sum_k v_k^{t+1}\phi_k\right)^2\right.\\&\left.+\left(\sum_k w_k^{t+1}\phi_k\right)^2\right\}\phi_i r_k^{t+1}dr^{t+1}\\&+\sum_{k=N_{a_l}}^{N_{a_{l+1}}}\mathfrak{L}\int_0^1\frac{\varphi^{t+1}-\varphi^t}{\Delta\tau}\phi_i\phi_k r_k^{t+1}dr^{t+1}.\end{aligned} \tag{45}$$

The material properties for the proceeding equations are:

$$\left.\begin{aligned}\kappa''(\varphi,\theta)&=\kappa_l''(\varphi,\theta)\\ \kappa'(\varphi,\theta)&=\kappa_l'(\varphi,\theta)\\ \overline{\rho C_p}&=\frac{\rho_l C_{p,l}}{\rho_0 C_{p,0}}\\ \bar{k}&=\frac{k_l}{k_0}\end{aligned}\right\}\quad r_l\le r\le r_{l+1}\quad l=1\ldots m \tag{46}$$

and

$$i=1\ldots N,\ j=1\ldots N_m\quad\text{and}\quad t=\text{time index.}$$

The implicit backward finite difference equations, used to discretize the time domain, result in an unconditionally stable algorithm. The residual equations (Eqs. 42, 43, 44 and 45) form a set of nonlinear algebraic equations. These are solved, using a Newton-Raphson scheme for the coefficients of the expansions in Eq. 41. If N is the total number of nodes, N_m (the number of the nodes in the mushy region), M (the number of fronts), and K either 0 or 1 for the absence or presence of a mushy region, the formulation yields a $(3N+M+KN_m\times 3N+M+KN_m)$ system:

$$\boldsymbol{J}(\boldsymbol{u}^{n,t+1})[\boldsymbol{u}^{n,t+1}-\boldsymbol{u}^{n+1,t+1}]=\boldsymbol{R}(\boldsymbol{u}^{n,t+1}), \tag{47}$$

where n is the Newton iterate index and t the time index. Equation 47 is solved at each time step. The Jacobian matrix $\boldsymbol{J}(\boldsymbol{u}^{n,t+1})$ contains the derivatives of the residual equations with respect to the unknowns, and $\boldsymbol{u}^{n,t+1}$ is the vector of unknowns and $\boldsymbol{R}(\boldsymbol{u}^{n,t+1})$ is the vector of the residuals. The temperature at a phase-change front is fixed, and its corresponding heat equation is replaced by a Dirichlet condition, $\theta_a=\theta_{\text{melt}}$. The entries that account for the heat transfer are placed in a row between the $R^{(3)}$ and $R^{(4)}$ to solve for the unknown front position. Thus, for two fronts there are two interior Dirichlet conditions and two extra rows and columns in the system. The extra column accounts for the derivative with respect to front position and the moving mesh. If a mushy region exists, the corresponding nodal temperatures are fixed in a similar manner and $R^{(4)}$ is added to the Jacobian matrix.

Table 1. Thermal Properties of the Frozen and Thawed Phases

Material Property	Water$_f^*$	Water$_t^{**}$
Heat capacity, C_p[W·s·kg^{-1}·°C^{-1}]	2,051	4,226
Thermal conductivity, k[W·m^{-1}·°C^{-1}]	2.22	0.56
Density, ρ[kg·m^{-3}]	1,000	1,000
Latent heat, λ[J·kg^{-1}]	3.34×10^5	

*Özişik (1980)
**Welty et al. (1976)

Physical parameters

Thermal properties in Table 1 are assumed to be independent of salinity. The density is assumed to be constant in all phases. Dielectric properties of ice and saline "sea" ice were taken from Mätzler and Wegmüller (1987). They presented a temperature-dependent equation for κ' (which was found to be virtually independent of frequency) and a frequency-dependent equation for κ'' with parameters dependent on temperature and impurity content. These relationships were used to find values of κ'' at -15°C and -5°C and were fit to a linear model for use in this study.

Pure and 0.1-M NaCl Ice: 915 MHz and 2,450 MHz

$$\kappa' = 3.19 + 9.1\times10^{-4}\ \mathrm{K}^{-1}(T - 273.15\ \mathrm{K}) \tag{48}$$

Pure Ice: 915 MHz

$$\kappa'' = 8.65\times10^{-4} + 3.0\times10^{-5}\ \mathrm{K}^{-1}(T - 273.15\ \mathrm{K}) \tag{49}$$

Pure Ice: 2,450 MHz

$$\kappa'' = 4.97\times10^{-4} + 1.66\times10^{-5}\ \mathrm{K}^{-1}(T - 273.15\ \mathrm{K}) \tag{50}$$

0.1-M NaCl Ice: 915 MHz

$$\kappa'' = 1.33 + 0.055\ \mathrm{K}^{-1}(T - 273.15\ \mathrm{K}) \tag{51}$$

0.1-M NaCl Ice: 2,450 MHz

$$\kappa'' = 0.80 + 0.036\ \mathrm{K}^{-1}\ (T - 273.15\ \mathrm{K}) \tag{52}$$

Kaatze (1989) analyzed the relative complex dielectric constant of pure water for temperatures between 0°C and 50°C and frequencies from 1.1 to 57 GHz. Kaatze fit these data to the Debye function to express frequency dependence and empirical nonlinear relationships to express temperature dependence:

$$\kappa^* = \kappa_\infty + \frac{\kappa_0 - \kappa_\infty}{1 + i\omega\tau} \tag{53}$$

where

$$\kappa_0 = 10^{1.94404 - 1.991\times10^{-3}\mathrm{K}^{-1}(T - 273.15)},$$

$$\kappa_\infty = 5.77 - 2.74\times10^{-2}\mathrm{K}^{-1}(T - 273.15),$$

and

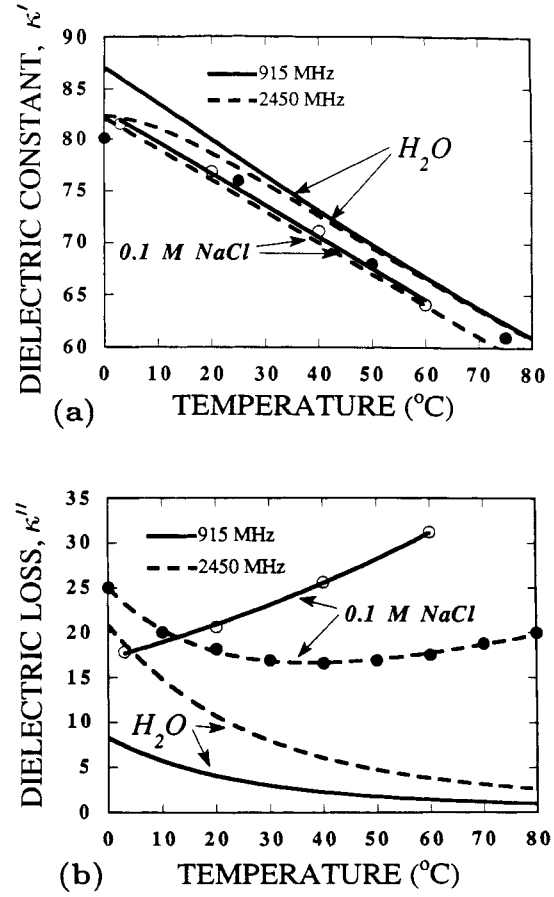

Figure 2. Relative dielectric constant for water (κ', 2a) (κ'', 2b) vs. temperature.

2a. Pure water at 915-MHz and 2,450-MHz values were calculated from Eq. 53 (Kaatze, 1989). Data taken from Ohlsson et al. (1974) are for 0.1-M NaCl at 900 MHz. Data taken from Mudgett (1986) are for 0.1 M NaCl at 2,450 MHz.

2b. Pure-water curves were calculated from Eq. 53 (Kaatze, 1989). Data taken from Ohlsson et al. (1974) are for 0.1-M NaCl at 900 MHz. Data taken from Mudgett (1986) are for 0.1-M NaCl at 2,450 MHz.

$$\tau = (3.745\times10^{-15}\ \mathrm{s})[1 + (7\times10^{-5}\ \mathrm{K}^{-2}) \times (T - 300.65\ \mathrm{K})^2]\exp(2.2957\times10^3\ \mathrm{K}/T).$$

The dielectric properties for 0.1-M NaCl were taken from Ohlsson et al. (1974) at 900 MHz and Mudgett (1986) for 2,450 MHz. Their experimental values were fit to a linear model, Eqs. 54 and 56, and values from Ohlsson et al. were used for the 915-MHz calculations.

Figure 2a shows the thawed state dielectric constant vs. temperature for 915 MHz and 2,450 MHz. There is little variation in κ' with respect to salt content and frequency. Dielectric loss data from Ohlsson et al. and Mudgett were fit to an exponential model, Eq. 55, and linear plus exponential model, Eq. 57, respectively. Figure 2b shows the variation in thawed state dielectric loss with respect to temperature. The dielectric loss

increases with salt content and decreases with respect to frequency and temperature for pure water. At 0.1-M NaCl and $f=915$ MHz, the loss increases with temperature, while at 2,450 MHz there is an initial decrease followed by a steady increase for temperatures greater than 40°C.

0.1-M NaCl at 915 MHz

$$\kappa' = 82.8 - 0.30\ \mathrm{K}^{-1}(T - 273.15\ \mathrm{K}) \tag{54}$$

$$\kappa'' = 17.1\exp[0.01\ \mathrm{K}^{-1}(T - 273.15\ \mathrm{K})] \tag{55}$$

0.1-M NaCl at 2,450 MHz

$$\kappa' = 82.1 - 0.30\ \mathrm{K}^{-1}(T - 273.15\ \mathrm{K}) \tag{56}$$

$$\kappa'' = 8.8 + 0.13\ \mathrm{K}^{-1}(T - 273.15) + 16.1\exp[-0.046\ \mathrm{K}^{-1}(T - 273.15\ \mathrm{K})] \tag{57}$$

Initial condition

To start the calculations, an initial front position and temperature profile were assumed. A single front was started at 99% of the radius. The temperature in the liquid layer was set at 273.15 K, and the frozen region was set at 253.15 K unless stated otherwise. The ambient temperature was 293.15 K and $h=20\ \mathrm{W\cdot m^{-2}\cdot K^{-1}}$. The Biot number was increased to $25Bi$ for the first 25 time steps to insure a positive flux of heat into the system that stabilized the initial motion of the thawing front. The effect of the final thawing time was minimal since the initial time step was $O\sim 0.01$ s and $T_a=293.15$ K: that is, microwave power was the main driving force for thawing. The equation that allowed for partial thawing of the frozen region was added when its average temperature exceeded 273.15 K.

In the two front situations, the second front was added when the center temperature exceeded 273.15 K or when the frozen fraction decreased below 0.05. The first element of the frozen region was divided in half with the inner half becoming the new, 12-element, liquid region.

All calculations were stopped when the front position reached 0.5% of the radius (for a single front) or when the frozen fraction decreased below 0.005. For the two fronts, the calculation was stopped when the difference between the fronts was within 0.5% of the radius.

Convergence criteria

Quadratic basis functions with three nodes per element and 12 elements per region were used. The time step was adjusted as a function of the first iterate error. The time step was limited to a maximum value (1 s to 5 s) which became smaller as the front(s) approached the termination criteria. The Newton iteration was terminated when

$$\sqrt{\frac{\sum_{i=1}^{3N+M+KN_m}(u_i^n - u_i^{n+1})^2}{3N+M+KN_m}} < 10^{-5}. \tag{58}$$

In general, convergence was achieved within five iterations.

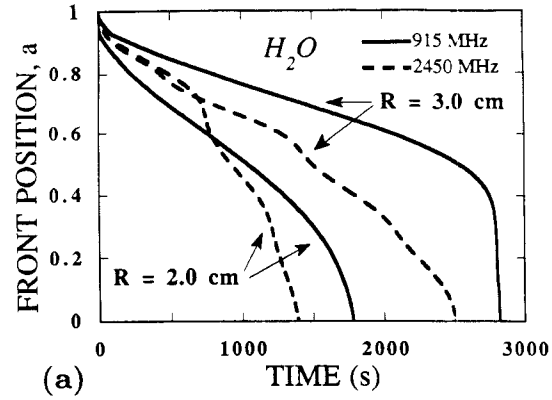

Figure 3a. Variation in front position with respect to time for pure ice/water cylinders: $f=915$ MHz and 2,450 MHz and $P_o=1.86\times10^4\ \mathrm{W\cdot m^{-2}}$.

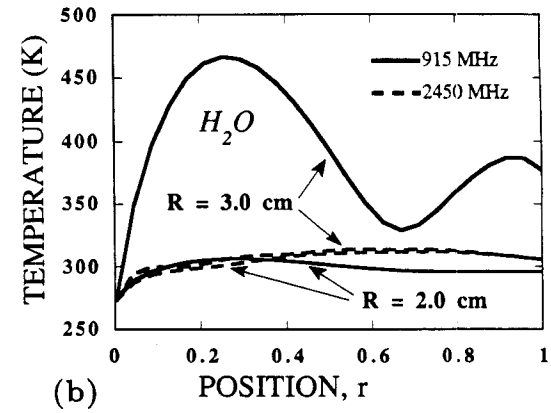

Figure 3b. Final temperature and dimensionless power vs. dimensionless position: $R=2.0$ and 3.0 cm.

Results and Discussion

Thawing simulations were performed for three different radii and several incident power levels at 915 MHz and 2,450 MHz. Both pure water and 0.1-M NaCl ice/water systems were considered.

Simulations for a pure-water system, $T_{0,f}=253.15$ K

The dimensionless front position is plotted vs. time in Figure 3a for $R=2.0$-cm and 3.0-cm cylinders exposed to 915-MHz and 2,450-MHz radiation and $P_o=1.86\times10^4\ \mathrm{W\cdot m^{-2}}$. Since pure ice is nearly lossless ($\kappa''\sim10^{-3}$), there is no mushy region (φ remained greater than 0.99 throughout the calculations) and the thawing process is governed by the dielectric properties of the thawed state. The thawing times for $P_o=0\ \mathrm{W\cdot m^{-2}}$ are 4.6×10^3 s and 9.8×10^3 s for the two radii. Thus, the thawing times are reduced by more than 50% for $f=915$ MHz and more than 70% for $f=2{,}450$ MHz. The "wavy" nature of the 2,450 MHz curves is due to resonance that occurs when λ_m is a harmonic of R. At resonance, power deposition increases, temperature increases, and the thawing front accelerates. Changes in temperature and front position effect λ_m, and eventually resonance subsides. Resonance, however, may occur several times throughout the thawing process. At 915 MHz

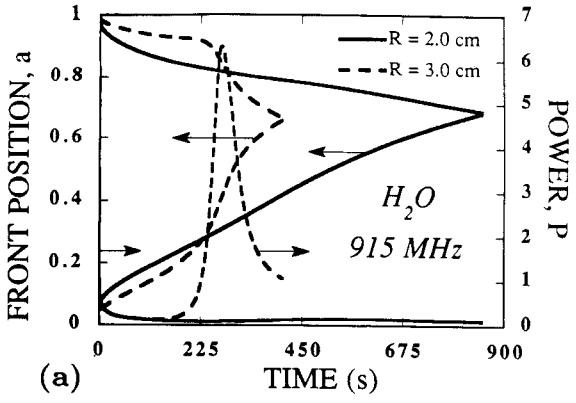

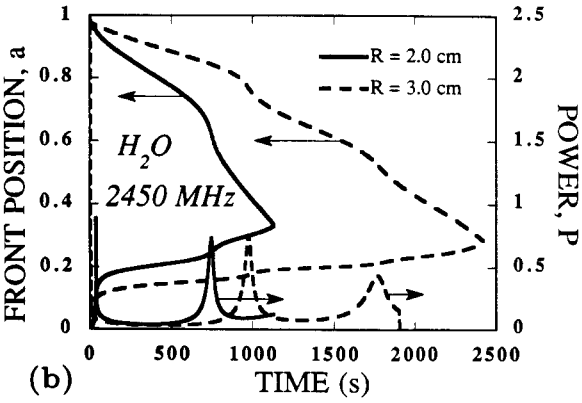

Figure 4. Variation in front position and dimensionless power deposition with respect to time at $P_o = 1.86 \times 10^4$ W·m^{-2}: 4a. $f = 915$ MHz; 4b. 2,450 MHz.

The power peaks due to resonance effects correspond to periods of rapid thawing.

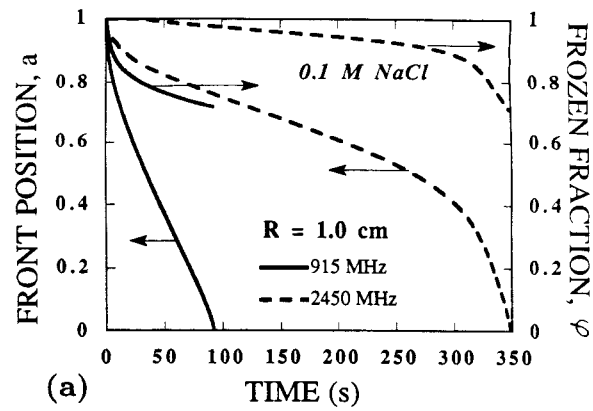

Figure 5a. Variation in front position and frozen fraction with respect to time for $f = 915$ MHz and 2,450 MHz.

The radius is 1.0 cm and incident power 1.86×10^4 W·m^{-2}.

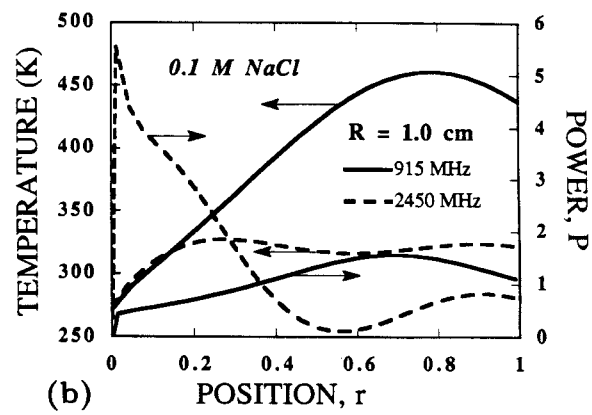

Figure 5b. Final temperature and dimensionless power vs. dimensionless position for $R = 1.0$ cm.

and $R = 3.0$ cm, resonance occurs only once near $t = 3.0 \times 10^3$ s. Note the rapid acceleration in the thawing front, from $r = 0.4$ to $r = 0.005$ in about 500 s ($\sim 1/7$th of the total thawing time).

The final temperature profiles are shown in Figure 3b. There is little variation for three of the cases.

Simulations for a pure-water system, $T_{0,f} = 273.10$ K

Simulations for $T_{0,f} = 273.10$ K demonstrates a situation with two fronts due to resonance. For a cylinder whose initial temperature is just below the melting point, focusing might cause the temperature at the center to rise more quickly than in the rest of the frozen region and a second thawing front is added when the center temperature exceeds 273.15 K.

Figure 4a shows the position of both thawing fronts and the total power deposition with respect to time for $f = 915$ MHz, $R = 2.0$ cm and 3.0 cm, and $P_o = 1.86 \times 10^4$ W·m^{-2}. The thawing time for the larger sample is 3,325 s and for the smaller cylinder is 2,340 s. Here, the resonance is not strong enough to open a front at the sample center.

For $f = 2{,}450$ MHz, resonance occurs twice for $R = 2.0$ cm and four times for $R = 3.0$ cm, see Figure 4b. The thawing times are 1.126×10^3 s and 1.522×10^3 s for $R = 2.0$ cm and 3.0 cm. The $R = 3$ cm cylinder initially at 253.15 K with one front thaws slower than the cylinder initially at 273.10 K with two fronts. For the $R = 3$ cm cylinder, resonance at the sample center causes a second front to be opened up at the start of thawing. This is seen by examining the power in Figure 4b. This, however, was not observed for the 2-cm cylinder.

Simulations for a 0.1-M NaCl system, $T_{0,f} = 253.15$ K

The dielectric loss of 0.1-M NaCl ice is $\sim 1{,}500$ times greater than the dielectric loss of pure ice. Therefore, power deposition in the frozen region is significant. For $R = 1.0$ cm and $P_o = 1.86 \times 10^4$ W·m^{-2}, mushy regions exist for $f = 915$ MHz and 2,450 MHz, see Figure 5a. The longer wavelength radiation thaws the cylinder in about 2/3 of the time required for the short wavelength radiation. Figure 5b shows the final temperature and power profiles. The power profiles reflect the characteristics of λ_m and indicate the occurrence of resonant conditions.

For $f = 915$ MHz and $R = 2.0$ cm, the results are similar to those for $R = 1.0$ cm: there is one front and the center core becomes mushy within the first 50 s (Figure 6a). At 2,450 MHz, the frozen fraction at the center decreases below 0.05 during a resonant period at $t \sim 150$ s and a second front is added. This inner front progress rapidly since the frozen fraction at the front is small. The front deccelerates as it moves toward regions

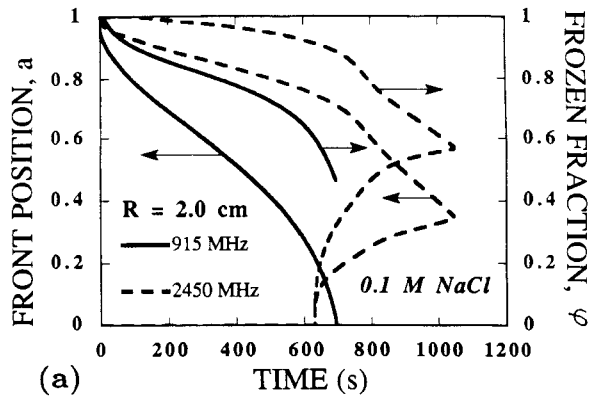

Figure 6a. Variation in front position and frozen fraction with respect to time for $f = 915$ MHz and 2,450 MHz.

The radius is 2.0 cm and incident power 1.86×10^4 W·m^{-2}.

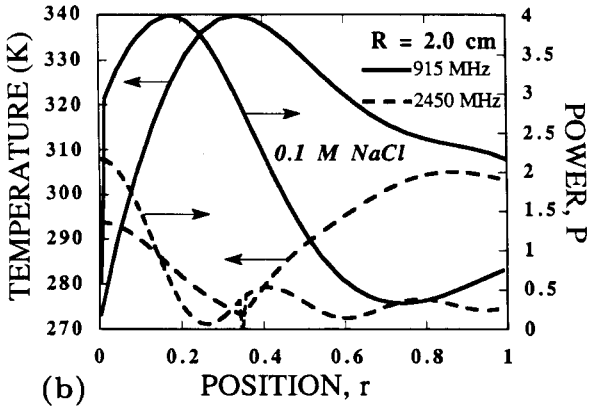

Figure 6b. Final temperature and dimensionless power vs. dimensionless position for $R = 2.0$ cm.

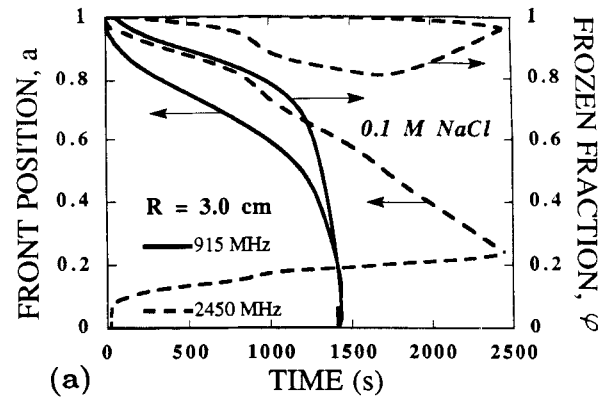

Figure 7a. Variation in front position and frozen fraction with respect to time for $f = 915$ MHz and 2,450 MHz.

The radius is 3.0 cm and incident power 1.86×10^4 W·m^{-2}.

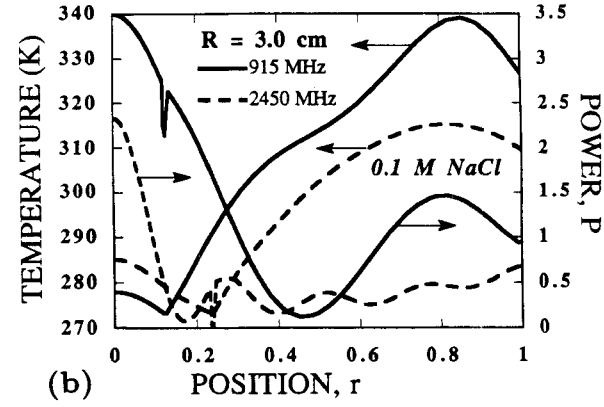

Figure 7b. Final temperature and dimensionless power vs. dimensionless position for $R = 3.0$ cm.

with a higher frozen fraction. The outer and inner front meet at $r \sim 0.4$ where $\varphi \sim 0.6$ in the last remaining fraction of mushy region.

The temperature and power profiles at the end of thawing are shown in Figure 6b. The temperature is lower at the center, a consequence of the second thawing front for the $f = 2{,}450$ MHz case. Additionally, $R < \lambda_m < 2R$ for $f = 915$ MHz and $\lambda_m \sim R/3$ for $f = 2{,}450$ MHz. Therefore, resonance occurs in the sample exposed to 2,450 MHz radiation only.

Two thawing fronts are needed at both wavelengths for the $R = 3.0$-cm cylinder simulations (Figure 7a). For $f = 2{,}450$ MHz, the inner front is initiated before the annular frozen region becomes mushy. This is due to focusing which causes the center temperature to rise above 273.15 K. The second front is added during the 915-MHz simulation when $\varphi(0) < 0.05$. This occurs during a resonant period in the final 50 s of the thawing process.

The final temperature and power profiles reflect the location where the difference between the two fronts is within 0.5% of R. The temperature in this thin mushy region is fixed at 273.15 K and φ is not quite 0. This causes a "divet" in the power profile since the power deposition is less than in the thawed region.

In regard to runaway heating, refer to Figure 2b (dielectric loss vs. temperature for 0.1-M NaCl at 2,450 MHz). If the center temperature does not rise above 40°C (313.15 K), runaway heating will not occur. Runaway heating occurs only when the dielectric loss increases with increasing temperature. The inward movement of the outer thawing front also reduces the amount of power deposited at the center. Energy deposited at the center must be dissipated as latent heat, whereas in the outer layer, heat is also lost to the surrounding environment when $T_s > T_a$.

These results are summarized in Figure 8 as total thawing time vs. incident power. The longer-wavelength, 915-MHz radiation thaws the $R = 1$ cm cylindrical samples more quickly given the same incident power than the 2,450-MHz radiation. For $R = 2$ cm and $R = 3$ cm where two fronts form at 2,450 MHz, the samples thaw faster at the same incident power than the 915-MHz radiation. The thawing time is a function of many parameters as illustrated by these simulations, most importantly, dielectric loss and λ_m in comparison to R.

Compared to the pure-ice/water system, the 0.1-M NaCl system thaws in a shorter time period and the time difference is greater for $f = 915$ MHz than for $f = 2{,}450$ MHz. For example, the $R = 2.0$ cm, 0.1-M NaCl cylinder thawed in 1,192 s when exposed to 915-MHz radiation, $P_o = 1.86 \times 10^4$ W·m^{-2} and the pure-water cylinder thawed in 2.406×10^3 s, a 50.5% reduction. For $R = 3.0$ cm, the times were 1.801×10^3 s and

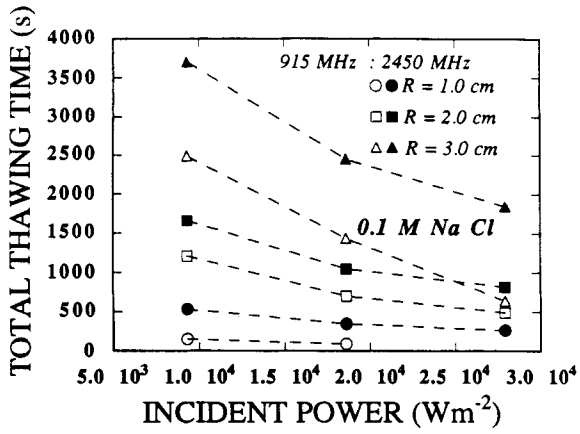

Figure 8. Total thawing time vs. incident power for the 0.1-M NaCl system.

3.502×10^3 s, a 48.5% reduction. Examining these same cases where $f = 2{,}450$ MHz and 0.1-M NaCl, thawing times were 869 s and 1.346×10^3 s for $R = 2.0$ cm and 3.0 cm, while pure-water cylinders thawed in 1.224×10^3 s and 1.556×10^3 s, corresponding to 29% and 13.5% reductions in thawing times.

Summary

The results presented here demonstrate phenomena that were not found in previous modeling efforts. Particularly, thawing from the "inside-out" and resonance effects. The first situation is a consequence of center focusing, while the latter occurs when λ_m is a harmonic of R. The realization of these phenomena is influenced strongly by the sample's dielectric properties. Additionally, our results show that samples with a higher κ'' thaw more quickly. Overall, these results have not been verified by experimental evidence, although it is expected that the conclusions drawn here will aid in the design and operation of microwave thawing and cooking processes.

Acknowledgment

The authors acknowledge Kraft General Foods Inc. for financial support, Simon Brandon for thoughtful discussions, and the Minnesota Supercomputer Institute for computing resources.

Notation

a = dimensionless front position
B = magnetic induction, $\mathrm{Wb \cdot m^{-2}}$
Bi = Biot number
c = velocity of light, $\mathrm{m \cdot s^{-1}}$
C_p = specific heat capacity, $\mathrm{J \cdot kg^{-1} \cdot K^{-1}}$
D = electric displacement, $\mathrm{C \cdot m^{-2}}$
E = electric field intensity, $\mathrm{V \cdot m^{-1}}$
f = frequency of incident radiation, Hz
h = heat transfer coefficient, $\mathrm{W \cdot m^{-2} \cdot K^{-1}}$
H = magnetic field intensity, $\mathrm{Amp \cdot m^{-1}}$
J = current flux, $\mathrm{Amp \cdot m^{-2}}$
k = thermal conductivity, $\mathrm{W \cdot m^{-1} \cdot K^{-1}}$
k_0 = reference thermal conductivity, $\mathrm{W \cdot m^{-1} \cdot K^{-1}}$
L = half length of sample, m
$\mathcal{L}$ = dimensionless latent heat
p = microwave source term, $\mathrm{W \cdot m^{-3}}$
P = dimensionless microwave source term
r = dimensionless radial distance
R = sample radius, m
s = front position, m
S = Poynting vector, $\mathrm{W \cdot m^{-2}}$
t = time, s
T = temperature, K
u = dimensionless electric field intensity
v = dimensionless real field component
w = dimensionless imaginary field component

Greek letters

α = wave number, $\mathrm{m^{-1}}$
α_0 = free space wave number, $\mathrm{m^{-1}}$
β = attenuation constant, $\mathrm{m^{-1}}$
γ = ratio of thermal diffusivity
δ = Kronecker delta
ϵ = permittivity, $\mathrm{F \cdot m^{-1}}$
ϵ_0 = free space permittivity, $\mathrm{F \cdot m^{-1}}$
ϵ' = dielectric constant, $\mathrm{F \cdot m^{-1}}$
ϵ'' = dielectric loss factor, $\mathrm{F \cdot m^{-1}}$
θ = dimensionless temperature
κ = relative permittivity
κ' = relative dielectric constant
κ'' = relative dielectric loss
λ = latent heat, $\mathrm{J \cdot kg^{-1}}$
λ_m = wavelength in medium, m
μ = permeability, $\mathrm{H \cdot m^{-1}}$
μ_0 = free space permeability, $\mathrm{H \cdot m^{-1}}$
ρ = density, $\mathrm{kg \cdot m^{-3}}$
ρ_0 = reference density, $\mathrm{kg \cdot m^{-3}}$
σ = electric conductivity, $\mathrm{mho \cdot m^{-1}}$
τ = dimensionless time
ϕ = basis functions
φ = frozen volume fraction
ω = angular frequency, $\mathrm{Rad \cdot s^{-1}}$

Subscripts

f = frozen phase
l = layer
m = number of layers in composite
M = number of fronts
t = thawed phase

Superscripts

n = Newton iterate index
t = time index

Literature Cited

Ayappa, K. G., H. T. Davis, G. Crapiste, E. A. Davis, and J. Gordon, "Microwave Heating: An Evaluation of Power Formulations," *Chem. Eng. Sci.*, **46**, 1005 (1991).

Ayappa, K. G., H. T. Davis, E. A. Davis, and J. Gordon, "Analysis of Microwave Heating of Materials with Temperature Dependent Properties," *AIChE J.*, **37**, 313 (1991).

Balanis, C. A., *Advanced Engineering Electromagnetics*, Wiley, New York (1989).

Coleman, C. J., "The Microwave Heating of Frozen Substances," *Appl. Math. Modelling*, **14**, 439 (1990).

Datta, A. K., "Heat and Mass Transfer in the Microwave Processing of Food," *Chem. Eng. Prog.*, **86**, 47 (1990).

Kaatze, U., "Complex Permittivity of Water as a Function of Frequency and Temperature," *J. Chem. Eng. Data*, **34**, 371 (1989).

Klassen, W., "Attenuation and Reflection of Radio Waves by a Melting Layer of Precipitation," *IEE Proc. Pt. H*, **137**, 39 (1990).

Mätzler, C., and U. Wegmüller, "Dielectric Properties of Fresh-Water Ice at Microwave Frequencies," *J. Phys. D: Appl. Phys.*, **20**, 1623 (1987).

Mudgett, R. E., "Electrical Properties of Foods," *Engineering Properties of Foods*, M. A. Rao and S. S. H. Rizvi, eds., Marcel Decker, New York (1986).
Ohlsson, T., N. E. Bengtsson, and P. O. Risman, "The Frequency and Temperature Dependence of Dielectric Food Data as Determined by a Cavity Perturbation Technique," *J. Microw. Pwr.*, **9**, 129 (1974).
Osepchuk, J. M., "A History of Microwave Heating Applications," *IEEE Trans. MTT*, **32**, 1200 (1984).
Özişik, M. N., *Heat Conduction*, p. 397, Wiley, New York (1980).
Pangrle, B. J., K. G. Ayappa, E. Sutanto, H. T. Davis, E. A. Davis, and J. Gordon, "Microwave Thawing of Semi-Infinite Slabs," *Chem. Eng. Comm.*, submitted (1991).
Pearce, J., "Why an Allocated ISM Frequency Near 900 MHz is Essential," *J. Microw. Pwr.*, **25**, 66 (1990).
Sihvola, A., "Macroscopic Permittivity of Dielectric Mixtures with Applications to Microwaves Attenuation of Rain and Hail," *IEE Proc. Pt. H*, **136**, 24 (1989).
Stratton, J. A., *Electromagnetic Theory*, McGraw-Hill, New York (1941).
Taoukis, P., E. A. Davis, H. T. Davis, J. Gordon, and Y. Talmon, "Mathematical Modeling of Microwave Thawing by the Modified Isotherm Migration Method," *J. Food Sci.*, **52**, 455 (1987).
Vant, M. R., R. O. Ramseier, and V. Makios, "The Complex-Dielectric Constant of Sea Ice at Frequencies in the Range 0.1–40 GHz," *J. Appl. Phys.*, **49**, 1264 (1978).
Varey, P., "Penetrating Arguments for Microwave Heating," *The Chem. Eng.*, **5**(10), 17 (1990).
Welty, J. R., C. E. Wicks, and R. E. Wilson, *Fundamentals of Momentum Heat and Mass Transfer*, Wiley, New York (1976).

Manuscript received May 17, 1991.